# Bulk transport properties of bismuth selenide thin films grown by magnetron sputtering approaching the two-dimensional limit

Yub Raj Sapkota, and Dipanjan Mazumdar

---

**Articles you may be interested in**

Bipolar resistive switching behavior in MoS$_2$ nanosheets fabricated on ferromagnetic shape memory alloy
Applied Physics Letters **112**, 262106 (2018); 10.1063/1.5037139

Impact of the ferroelectric layer thickness on the resistive switching characteristics of ferroelectric/dielectric structures
Applied Physics Letters **113**, 102904 (2018); 10.1063/1.5047853

Light-induced magnetization changes in aggregated and isolated cobalt ferrite nanoparticles
Journal of Applied Physics **124**, 103904 (2018); 10.1063/1.5040327

Multiband light emission and nanoscale chemical analyses of carbonized fumed silica
Journal of Applied Physics **124**, 105108 (2018); 10.1063/1.5042671

Large negative anisotropic magnetoresistance in Co$_2$MnGa Heusler alloy epitaxial thin films
Applied Physics Letters **113**, 112407 (2018); 10.1063/1.5047821

Investigation of the prebreakdown stage of the self-sustained subnanosecond discharge in high pressure nitrogen
Journal of Applied Physics **124**, 103304 (2018); 10.1063/1.5024974

---

# Bulk transport properties of bismuth selenide thin films grown by magnetron sputtering approaching the two-dimensional limit

Yub Raj Sapkota and Dipanjan Mazumdar

*Physics Department, Southern Illinois University, 1245 Lincoln Drive, Carbondale, Illinois 62901, USA*

Transport properties of topological insulator $Bi_2Se_3$ thin films are investigated with an emphasis on understanding finite-size effects as the two-dimensional limit is approached. Ultra-smooth, (000*l*)-oriented $Bi_2Se_3$ thin-films fabricated using radio-frequency magnetron sputtering reveal disproportionately large changes in bulk resistivity and Hall mobility below six quintuple layers (QL). We correlate such changes to the bulk (other than surface) electronic structure where a bandgap enlargement is observed below six QL in optical absorption spectroscopy measurements. This effect is strongest at the three and two quintuple layers that show the largest changes in bandgap. Temperature dependent transport measurements reveal the effect of disorder from substrate and high carrier concentration. Films on sapphire substrate demonstrate better transport properties compared to amorphous quartz. While temperature dependence of bulk resistivity is both thickness and substrate sensitive, the temperature dependence of Hall coefficient is determined only by the carrier concentration in films. Our work highlights the influence of the bulk electronic structure on the transport properties of few-layer $Bi_2Se_3$ which is of interest in the applied areas of optoelectronics, nanoelectronics, and spintronics. *Published by AIP Publishing.* https://doi.org/10.1063/1.5018856

## I. INTRODUCTION

Topological insulators (TIs) are a new class of matter with bulk insulating states combined with topologically protected metallic surface states.[1,2] Experimental realization of 3D topological states at room temperature and in the absence of an external magnetic field has widened the interest of such materials beyond condensed matter physics.[3–6] Apart from applications in spintronics and fault-tolerant quantum computing,[7–11] topological states are now considered for a variety of applications such as interconnects[12] and low-power electronics.[13] In this respect, the useful material properties must survive various tests of scalability and compatibility. Therefore, understanding the properties of TIs in the two-dimensional limit will provide the platform for future investigations regarding their applications.

Bismuth selenide ($Bi_2Se_3$) is the prototypical topological insulator material. Discovery of single Dirac cone[4] at the Brillouin zone center in $Bi_2Se_3$ has fueled tremendous interest in the research community. It is also a recognized thermoelectric material with a relatively small bandgap (0.3 eV in bulk form). Therefore, $Bi_2Se_3$ is an ideal system for exploratory investigations regarding the application of TIs. Various thin-film growth methods can be employed to grow TI materials. High-quality $Bi_2Se_3$ films down to 2 quintuple layers (QL) has been established using Molecular Beam Epitaxy (MBE) method on sapphire,[14–16] whereas properties on Si,[17–19] $SiO_2$,[20] GaAs,[21] and other underlayers[22,23] have also been investigated.[24] Other growth methods are also gaining attention such as Pulsed laser deposition (PLD),[25,26] chemical vapor deposition[27] and magnetron sputtering.[28,29] From an application point of view, magnetron sputtering is highly versatile and a well-established method for growing a variety of heterostructures in applied areas such as

spintronics. Therefore, investigation of TI materials grown using magnetron sputtering is relevant.

Investigation of transport properties is of paramount importance to properly utilize the conducting surface states for device applications. Single crystal and thin-film $Bi_2Se_3$ are prone to high bulk carrier concentration, irrespective of growth method. The high carrier concentration is also induced by mechanical exfoliation,[30] and exposure to ambient conditions.[31,32] Studies show that chemical doping,[33,34] electrochemical doping[30] and synthesis in Se-rich conditions[35] can lower the bulk carrier concentration in $Bi_2Se_3$. But as many recent investigations reveal, high carrier concentration samples do not necessarily preclude investigations and application of TIs.[36–39]

This work is focused on investigating the transport properties of $Bi_2Se_3$ thin films grown using radio-frequency magnetron sputtering method and understand the variation of carrier concentration, resistivity, and mobility as the two-dimensional limit is approached (few-layer properties). Hall measurements reveal high bulk carrier concentration in all films irrespective of thickness and substrate. Bulk resistivity and Hall mobility values show disproportionately large variation with reduced thickness that is consistent with prior reports on MBE grown thin-films[14–17] and few-layer single crystal.[40] Leveraging on our prior work, where we demonstrated optical blue-shift in few-layer $Bi_2Se_3$ compared to bulk,[29] we correlate the higher resistivity and reduced mobility behavior at the few-layer level directly to the increase in the bulk bandgap of $Bi_2Se_3$. We also show that the choice of the substrate can strongly influence transport properties through film-substrate disorder as the conductivity, and mobility values as a result, of films are lower on amorphous quartz compared to crystalline $Al_2O_3$. Overall, we highlight

several interesting properties of few-layer $Bi_2Se_3$ for potential device applications.

## II. EXPERIMENTAL DETAILS

$Bi_2Se_3$ thin films was grown using commercially available stoichiometric target (Kurt Lesker, 99.999% purity) and RF sputtered in a high vacuum magnetron sputtering system (base pressure $\sim 4 \times 10^{-9}$ Torr). The growth rate was over 10–15 QL/min under moderate power conditions. Initially, many films were grown at room temperature and annealed in-situ at 300 C on various substrates such as $Si/SiO_2$ (100 nm), amorphous BN-buffered Si, (001)-oriented Si with a native $SiO_2$ layer, c-oriented $Al_2O_3$ (sapphire), and amorphous quartz ($SiO_2$). The crystal structure and interface quality using X-ray diffraction (XRD) and X-ray reflectivity (XRR) method were investigated using a high-resolution Rigaku Smartlab Diffractometer. Transport properties were evaluated primarily on quartz substrates to directly correlate with prior optical bandgap measurements of $Bi_2Se_3$ by the authors[29] and avoid spurious interference from substrates such as $Si/SiO_2$. Additional samples on sapphire substrates were fabricated to investigate substrate-induced disorder. Transport and Hall measurements were performed using a NanoMagnetics Instruments ezHEMS system in the Van-der-Pauw (VDP) geometry to obtain a vast range of parameters such as carrier-type, 2D and 3D carrier concentration, sheet resistance, bulk resistivity, and Hall mobility as a function of thickness and temperature. Measurements were performed on exposed thin films deposited on $1 \times 1$ cm substrates immediately after sample fabrication and repeated whenever necessary by making new samples. Four-probe ohmic contacts made by making light contacts with Au/Cr probes onto silver paint deposited at the corners of square samples provided linear I-V curves (see Figs. S1 and S2). Hall measurements were performed using 1–100 $\mu$A current (depending on sample resistance) and a constant low magnetic field (0.66 T) provided by a set of permanent magnets. Surface morphology of few-layer $Bi_2Se_3$ was evaluated using the atomic force microscopy (AFM) technique with a Park Scientific Auto-Probe CP AFM.

## III. RESULTS AND DISCUSSION

In Fig. 1(a), we show the X-ray reflectivity (XRR) pattern of approximately 10–12 QL $Bi_2Se_3$ films grown on different substrates. An oscillatory pattern is observed in all

cases, which indicates a sharp interface with the substrate. Analysis of the critical angle reveals that the measured film densities are higher than the bulk value of 6.8 g/cm$^3$ by about 15%–20%. Though this may be within the error margin of our measurement, it might also indicate the formation of a thin layer of $Bi_2O_3$ at the surface which has a higher density than $Bi_2Se_3$. Fits to the XRR data quantify the film roughness value. We observe that all films show less than 1 QL roughness regardless of the substrate. Particularly, the film on $Al_2O_3$ is virtually atomically smooth, while the film on Si/$SiO_2$ shows 0.45 nm rms roughness. The film on bare Si (with a native oxide layer) and amorphous-BN buffered Si show marginally higher but a comparable roughness of 0.9 and 0.7 nm, respectively. Such results demonstrate that atomically smooth substrates show better film morphology.

In Fig. 1(b), we show the high-resolution $\theta$-$2\theta$ X-ray diffraction scans of the films shown in Fig. 1(a). Only (000l) $Bi_2Se_3$ peaks are observed on all substrates apart from substrate peaks (indicated by "Sub") indicating out-of-plane (c-axis) growth in all cases. The film on $Al_2O_3$ (red) shows the highest intensity among all substrates whereas the film on amorphous BN (green) shows the lowest XRD intensity [by almost a factor of five for the (0006) peak]. The films on Si/$SiO_2$ and Si are of intermediate quality. Full-width-at-half-maxima (FWHM) values also show a similar trend. There is no significant difference in the out-of-plane lattice parameter which indicates that strain effect is not important for $Bi_2Se_3$, which is reasonable for a layered material. Taken together with X-ray reflectivity data, $Bi_2Se_3$ films on $Al_2O_3$ show the best structural and topographic characteristics, while films on amorphous substrates, particularly Si/$SiO_2$, are also promising. The structural behavior of sputtered samples is consistent with MBE grown thin-films.[14–21]

We conducted Atomic Force Microscopy (AFM) scans of films on quartz substrates (the samples used for transport measurements) that are not accessible via XRR. Figures 2(a) and 2(b) show 60 $\mu$m $\times$ 70 $\mu$m scans of the 2 and 3 QL films and Figs. 2(c) and 2(d) show their typical line scans. The films show near-atomic level smoothness with a sub-nanometer peak to valley profile without any noticeable discontinuity at the nanoscale level. Different areas of the samples demonstrate similar morphology. The RMS roughness is estimated to be 0.23 nm for the 2 QL film and 0.16 nm for the 3 QL film. Such values are consistent with XRR analysis on the Si/$SiO_2$ substrate. Optical and
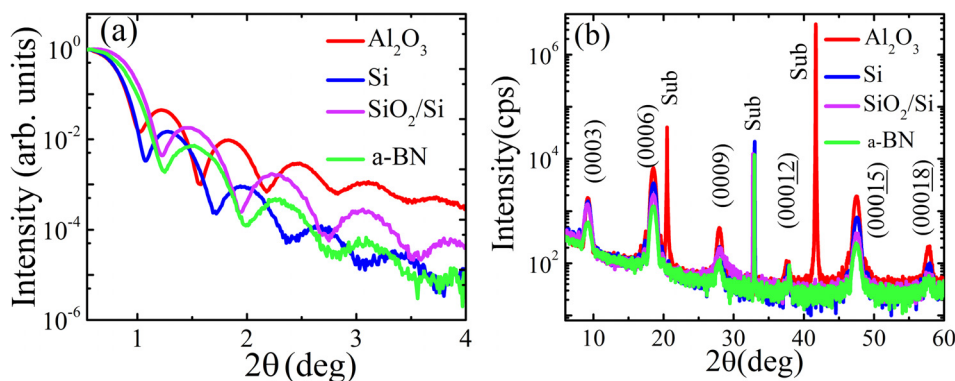


FIG. 1. (a) X-ray reflectivity of $Bi_2Se_3$ films deposited on different substrates as indicated. a-BN substrate implies amorphous BN grown on silicon substrate. (b) X-ray diffraction patterns of 10–12 nm $Bi_2Se_3$ films grown on different substrates. "Sub" indicated peaks from various substrates.
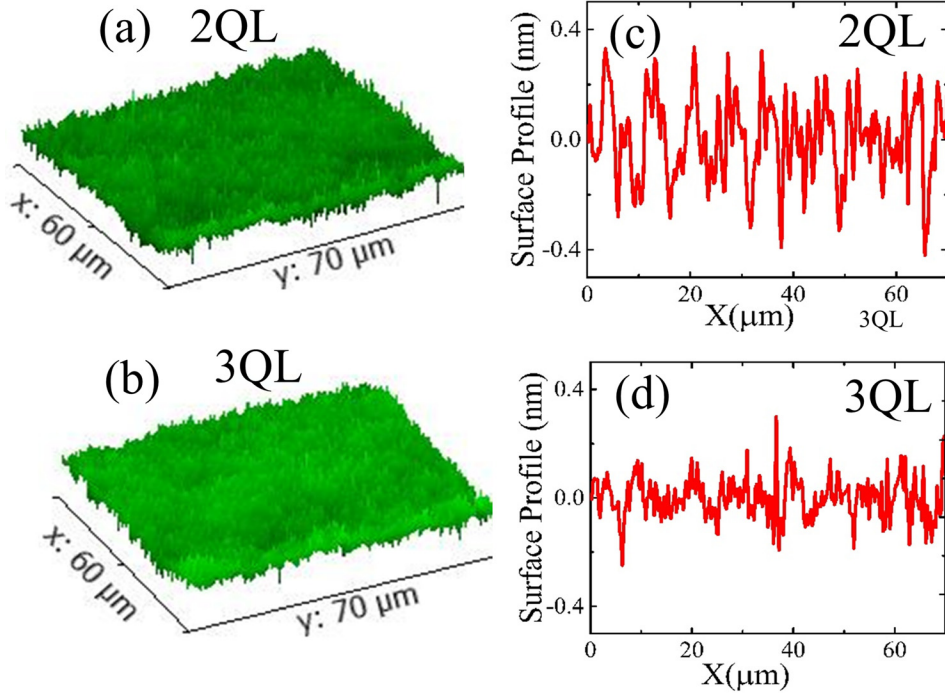
FIG. 2. Atomic-force microscopy scan of (a) 2 QL and (b) 3 QL $Bi_2Se_3$ thin film over a $60\,\mu m \times 70\,\mu m$ area. (c) and (d) Typical line scans of the data shown in (a) and (b).

photographic images also show uniform and thickness-consistent color (see Fig. S1). Therefore, all evidence shows that the films are ultra-smooth, and reliable transport measurements are possible down to the 2 QL level.

In Fig. 3, we describe the thickness dependent XRD measurements. Figure 3(a) shows the high-resolution XRD pattern of a 35 nm $Bi_2Se_3$ film deposited on the Si/SiO$_2$ substrate. Various (000l) peaks assigned to $Bi_2Se_3$ are clearly observed. The intensities are normalized with respect to the highest (0006) peak and compared to a simulated pattern[41] of bulk $Bi_2Se_3$[42] that is indicated by the black stars. As evident, apart from the excellent agreement in the Bragg peak, the experimental intensities match the simulated values for all but the (00015) peak. This indicates the growth of highly oriented, strain-free, $Bi_2Se_3$ films with a bulk-like crystal structure. The oriented crystal structure is also observed over a wide thickness range as shown in Fig. 3(b), where (000l) peaks are observed down to 6 QL. In Figs. S3 and S4 of the supplementary material, we plot the XRD data of the 4 nm $Bi_2Se_3$ on the sapphire and quartz substrate. It is reasonable to assume that the structural integrity is maintained in films lower than 4 QL as optical absorption spectroscopy

measurements show features consistent with a strong crystal structure down to 2 QL (see Fig. S5 and Ref. 29). We now shall discuss the transport properties of the characterized films on quartz substrates.

In Table I, we report the room temperature values of various transport properties for films on quartz substrates along with their optical bandgap as reported previously by the authors.[29] A close inspection reveals that thickness has a strong impact on various aspects of transport, particularly below 6 QL. Let us discuss them one by one. In Fig. 4(a), we show the variation of sheet carrier concentration ($n_{2D}$) with thickness. The data can be separated into two regimes as indicated by the two dashed straight lines for guidance. Between 90 and 6 QL, there is a slow monotonic reduction in 2D by about a factor of 2 or 3. However below 6 QL, we notice a much sharper reduction by a factor of 5–6 as the thickness approaches 2 QL. Specifically, $n_{2D}$ values for the 2, 3, 4, and 6 QL films are 1.8, 2.9, 6.0, and $9.8 \times 10^{13}$ cm$^{-2}$. Even though the values are of the same order of magnitude, the sharp monotonic drop is noteworthy in the context of electronic structure changes for a relatively small change in thickness.[29,43,44] Our data qualitatively agrees with reports
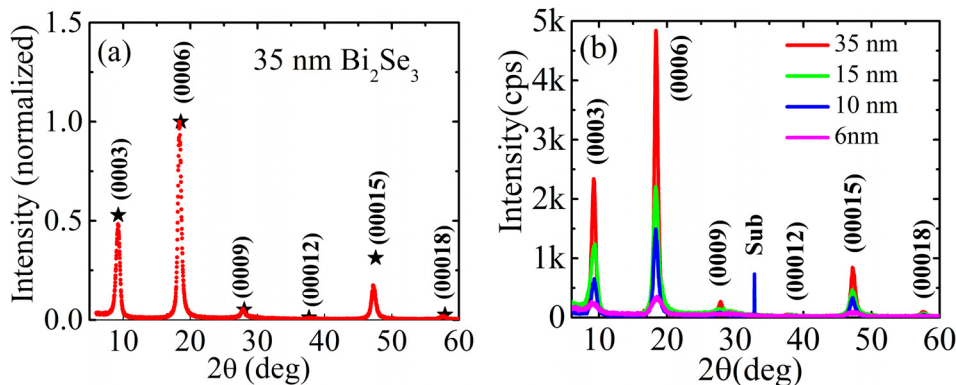


FIG. 3. (a) Normalized XRD pattern of a 35 nm $Bi_2Se_3$ film grown on Si/SiO$_2$ showing only (000l) Bragg peaks. Simulated XRD intensities corresponding to (000l) Bragg peaks are shown using black stars. A very good agreement is observed except for the (00015) peak. (b) XRD scans of $Bi_2Se_3$ thin films of different thicknesses as indicated. 'Sub' indicates substrate peak.

TABLE I. Room temperature carrier concentration (bulk and surface), bulk resistivity, and Hall mobility of $Bi_2Se_3$ thin films deposited on quartz substrate, along with their optical bandgap as reported in Ref. 29. N-type behavior was observed in all films.

| Thickness (nm) | Sheet concentration ($cm^{-2}$) | Bulk concentration ($cm^{-3}$) | Sheet resistance ($h/e^2$ ohm/sq) | Longitudinal resistivity (ohm.cm) | Hall mobility ($cm^2$/V s) | Optical band gap (eV)[29] |
|---|---|---|---|---|---|---|
| 90 | $4.2 \times 10^{14}$ | $4.72 \times 10^{20}$ | $4.66 \times 10^{-3}$ | $1.08 \times 10^{-3}$ | 122.02 | … |
| 25 | $2.46 \times 10^{14}$ | $9.83 \times 10^{19}$ | $9.50 \times 10^{-3}$ | $6.1 \times 10^{-4}$ | 103.00 | 0.46[a] |
| 15 | $1.64 \times 10^{14}$ | $1.09 \times 10^{20}$ | $2.09 \times 10^{-2}$ | $8.10 \times 10^{-4}$ | 70.45 | 0.47 |
| 6 | $9.76 \times 10^{13}$ | $1.63 \times 10^{20}$ | $1.00 \times 10^{-1}$ | $1.56 \times 10^{-4}$ | 24.61 | 0.52 |
| 4 | $6.02 \times 10^{13}$ | $1.50 \times 10^{20}$ | $2.58 \times 10^{-1}$ | $2.67 \times 10^{-3}$ | 15.54 | 0.58 |
| 3 | $2.90 \times 10^{13}$ | $9.60 \times 10^{19}$ | 1.79 | $9.2 \times 10^{-3}$ | 4.66 | 0.63 |
| 2 | $1.80 \times 10^{13}$ | $9.02 \times 10^{19}$ | 7.24 | $3.74 \times 10^{-2}$ | 1.86 | 0.82 |

[a]Bandgap of a 30 nm film.
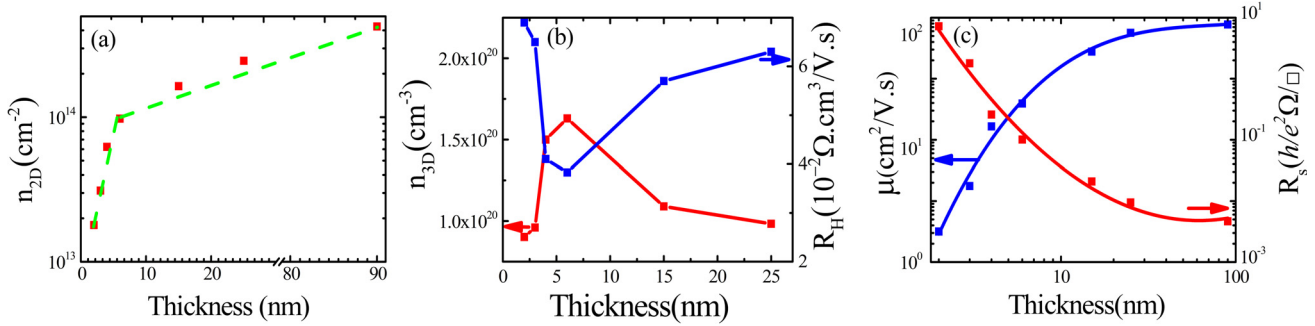


FIG. 4. (a) Variation of sheet carrier concentration ($n_{2D}$) with thickness in sputtered $Bi_2Se_3$ films. Raw data shown in Table I. The dashed line is drawn to serve as a guide. (b) Variation of bulk carrier concentration ($n_{3D}$) and Hall coefficient ($R_H$) as a function of thickness for $Bi_2Se_3$ films on quartz substrate at 300 K. (c) Variation of sheet resistance and Hall mobility as a function of film thickness.

on MBE grown samples[14–16] and compared in Table T1. Liu et al.[15] reported a carrier concentration of $(3.5 \pm 0.5) \times 10^{13} \, cm^{-2}$ in 1–6 QL films and mentioned the slight changes with thickness (but not quantified). Bansal et al.[14] reported $1.9 \times 10^{13} \, cm^{-2}$ for a 2 QL film, which is very close to our value. Similarly, Richardella et al.[21] reported a carrier concentration of $1.2 \times 10^{13} \, cm^{-2}$ for a 3 QL film which is also close to our report. A 6 QL sample grown with the PLD method is reported to have $n_{2D} = 1.3 \times 10^{14} \, cm^{-2}$.[26] The bulk carrier concentration ($n_{3D}$) follows a non-monotonic trend, and the values in the 2–25 QL range are plotted in Fig. 4(b). A consistent increase in the values is observed until 6 QL after which $n_{3D}$ sharply decreases for the 4, 3, and 2 QL films. This provides another evidence that the fundamental properties below 6 QL thickness, particularly at the 2 and 3-layer, are substantially different from thicker films. Since the carrier concentration is related to the Hall coefficient, $R_H = 1/ne$, $R_H$ shows a similar, but inverted, trend with thickness. We shall further discuss the implication of the Hall coefficient values in relation with mobility in Fig. 6.

The variation of sheet resistance ($R_s$) with thickness is shown in Fig. 4(c) in terms of $h/e^2 = R_k = 25.812 \, k\Omega$, the Von-Klitzing constant. $R_s$ decreases monotonically from $4.6 \times 10^{-3} \, R_k$ for the 90 QL film to $0.1 \, R_k$ at 6 QL, and over an order of magnitude change is observed from 6 to 2 QL level. Such a trend is qualitatively consistent with several reports of MBE samples on sapphire[14–16] where typically over an order of magnitude variation is observed between 6 and 2 QL. The sheet resistance values on quartz substrates reported here are higher compared to literature reports on

sapphire and is rationalized in terms of higher surface roughness on quartz relative to sapphire (see Figs. 1 and 2). The difference in $R_s$ values is marginal ($\sim$35%) when sputtered 4 QL films grown on sapphire are compared to high-quality MBE films[15] (see Tables T1 and T2).

Hall mobility values at room temperature also show large variations with thickness as shown in Fig. 4(c). Films thicker than 25 QL films show values over $100 \, cm^2$/V.s which sharply drops to $25 \, cm^2$/V.s at 6 QL level, and further to $4.7 \, cm^2$/V.s and $1.8 \, cm^2$/V.s at the 3 and 2 QL level, respectively. Qualitatively, the sharp drop in mobility values with decreasing thickness is reported in MBE samples grown on sapphire[14,15] as is shown in Table T1. Liu et al.[15] reported mobilities of $350 \, cm^2$/V.s and $31 \, cm^2$/V.s at 2 K for 6 and 2 QL samples on sapphire. Bansal et al.,[14] using a two-channel model, reported values of $50–60 \, cm^2$/V.s and $100–200 \, cm^2$/V.s for 2 and 4 QL samples on sapphire. In our case, a 4 QL film on sapphire shows a mobility of $43 \, cm^2$/V.s at 85 K (Table T1). Jeon et al.[20] reported a mobility of $5 \, cm^2$/V.s at 300 K on a 5 QL MBE sample on $Si/SiO_2$ and Onose et al.[26] reported a mobility of $10 \, cm^2$/V.s at 2 K on a PLD-grown 6 QL sample on InP. The comparison clearly shows that the mobility values of sputtered films compare favorably with other growth methods.

We interpret the variation of bulk resistivity and Hall mobility in terms of the measured optical bandgap values in Fig. 5. Previously, we showed that the bulk bandgap of $Bi_2Se_3$ blue-shifts by 0.3 eV as the thickness is reduced from 6 QL to 2 QL (Ref. 29 and Fig. S5), which is consistent with first-principles electronic structure calculations.[43,44] Our
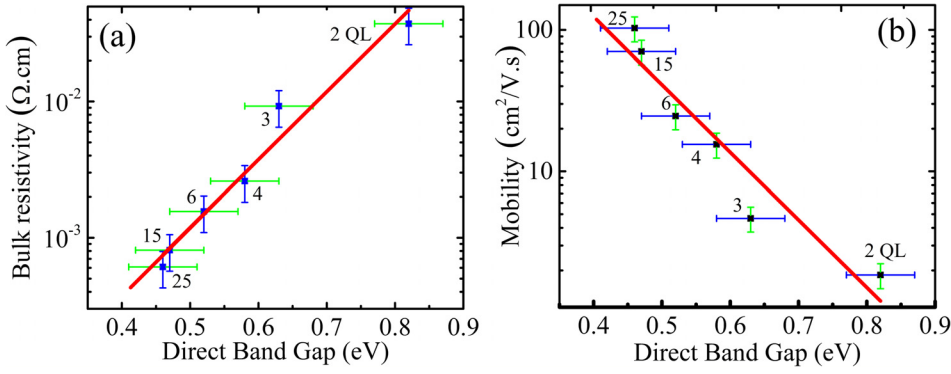
FIG. 5. Variation of (a) bulk resistivity (b) mobility in $Bi_2Se_3$ with measured optical bandgap from Ref. 29 and reproduced in Table I. Each data point corresponds to a specific film thickness as indicated.

optical measurements also found evidence of Burstein-Moss effect that accounted for an additional enlargement of 0.2 eV in all films. The Burstein-Moss effect explains why films thicker than 6 QL films do not show the 0.3 eV bulk value. As clearly shown in the figures, the variation in resistivity and Hall mobility strongly correlates with the measured bandgap. Films with a higher bandgap show higher resistivity and lower mobility. The scaling behavior of resistivity can be fitted to $\rho = Ae^{\beta E_g}$ ($E_g$ = bandgap) where $\beta = 11.49 \pm 1.08$ eV$^{-1}$, which is roughly equal to $(4 k_B T)^{-1}$ and about half the $(2 k_B T)^{-1}$ scaling factor of an intrinsic semiconductor. Since Hall mobility is related to the resistivity through the relation $\mu = R_H/\rho$, ($R_H$ = Hall coefficient = 1/ne), the reduced mobility in few-layer $Bi_2Se_3$ can be explained as due to the increase in resistivity which, in turn, as we argue is due to the increase in bandgap. Such behavior is reported in zero bandgap systems like graphene where the mobility reduces dramatically when a bandgap is induced.[45,46] Therefore, we find that the behavior of ultra-thin $Bi_2Se_3$ films is extremely sensitive to small changes in the bulk

bandgap which can be interesting for device applications. Our interpretation can also explain the scaling behavior observed across different growth methods.[14–16]

Extrinsic factors such as high carrier concentration, structural, and film-substrate disorder also play a strong role in transport. We performed temperature dependent measurements for different thicknesses and substrates to understand the role of such factors. In Figs. 6(a) and 6(b), the bulk resistivity and sheet resistance of 90, 15, and 4 QL $Bi_2Se_3$ films on quartz is shown as a function of temperature (85–295 K). Two trends are noteworthy besides an increase in values with reduced thickness. First is the linear metallic behavior ($d\rho_{xx}/dT$ is constant) in the entire temperature range that is attributed to strong electron-phonon scattering from high carrier concentration.[47] Second is the progressive decrease in the slope with reduced thickness. This could imply a crossover to an insulating behavior at low temperatures for thinner films, similar to several,[15,16] but not all,[14] reports on MBE films on sapphire. An insulating behavior is also reported in ultra-thin exfoliated $Bi_2Se_3$ single crystals by Cho et al.[40]
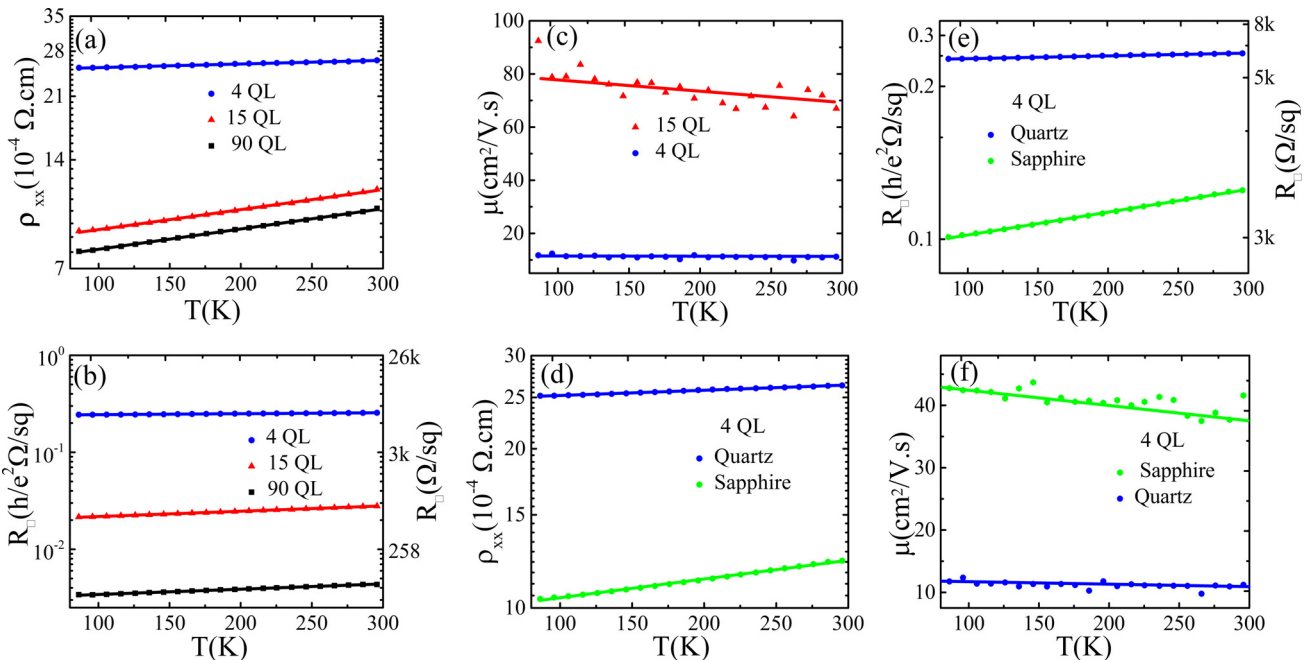


FIG. 6. (a) Resistivity and (b) sheet resistance of 4, 15, 90 QL $Bi_2Se_3$ deposited on a quartz substrate. (c) Hall mobility vs. temperature of 4 and 15 QL $Bi_2Se_3$ deposited on quartz. (d) Resistivity and (e) sheet resistance of a 4 QL film on quartz and sapphire. Sheet resistance is shown in terms of von-Klitzing constant and the nominal value for comparison. (f) Temperature variation of Hall mobility of a 4 QL film deposited on the quartz and sapphire substrate.

from FET measurements. Both bandgap enlargement and disorder promote insulating behavior, and it is difficult to quantify their contribution from temperature dependent behavior alone. But taken together with optical absorption results and the disproportionate variation as a function of thickness, we assert that intrinsic effects are playing a big role. Evidence to this end includes the following: (a) optical data below 6 QL do not show strong broadening effects; (b) ultra-smooth, continuous films keep disorder-related effects to a minimum.

In Fig. 6(c), we show the temperature dependence of Hall mobility for the 4 and 15 QL films on quartz. The mobility is essentially constant for the 4 QL film and somewhat stronger for the 15 QL film. Looking deeper, the Hall coefficient ($R_H$) is observed to be practically constant in the entire temperature range as shown in Fig. S6, which implies that the temperature dependence of Hall mobility is directly related to the change in resistivity with temperature. The insensitivity of Hall coefficient, and mobility to a large extent, to temperature as a function of thickness is attributed to high carrier concentration and consistent with the work of Butch et al.[48]

We have additionally fabricated $Bi_2Se_3$ films on sapphire substrates to directly understand the influence of disorder below 6 QL (see Table T2 for values at 300 K). In Figs. 6(d) and 6(e), we compare the temperature-dependence of bulk resistivity and the sheet resistance of a 4 QL $Bi_2Se_3$ film on sapphire and quartz. Comparison between films of same thickness is necessary to normalize the intrinsic effects. The resistivity of the 4 QL film is nearly double on quartz compared to sapphire. Also, the metallic behavior, as inferred from the slope in d$\rho$xx/dT curve, is stronger on sapphire. Both these data imply higher disorder on the quartz substrate. In Fig. 6(f), we compare the temperature dependence of Hall mobility in 4 QL $Bi_2Se_3$ deposited on sapphire and quartz. Again, both value and the slope are substantially different. The mobility values are 3–4 times higher on sapphire compared to quartz. This can be explained as almost equally due to higher conductivity [Fig. 6(d)] and higher Hall coefficient (see Fig. S7) of films grown on sapphire. The variation of Hall coefficient values, which is related to carrier concentration, is within the 30%–40% variation observed in samples of same thickness. The difference in the slope, however, originates almost exclusively from the change in resistivity and not Hall coefficient which is practically constant over the entire temperature range (see Fig. S7). Therefore, temperature dependence of Hall response does not show direct substrate or thickness dependence and controlled strongly by carrier concentration.

Combining thickness and substrate dependence with temperature, we show that transport properties of ultra-thin $Bi_2Se_3$ films are sensitive to extrinsic factors such as substrate-induced disorder scattering and electron-phonon scattering from high carrier concentration. The sapphire substrate provides a better lattice match and promotes low interface disorder with $Bi_2Se_3$ which translates to better transport properties. Tuning of growth conditions will reduce unwanted carriers. Implementation of such advances will allow the intrinsic bulk and surface properties to dominate.

## IV. CONCLUSION

Transport properties of ultra-smooth and high-quality $Bi_2Se_3$ thin-films fabricated using magnetron sputtering are investigated between 2 and 100 quintuple layer thickness. We show significant changes in bulk and surface carrier concentration along with disproportionately large enhancement in bulk resistivity values and concurrently strong reduction in Hall mobility in films below 6 QL. Using complementary optical absorption measurements, we demonstrate that the variation in transport properties is consistent with an enlargement of the bulk bandgap of $Bi_2Se_3$. Temperature-dependent measurements show that both substrate and thickness have a strong impact on resistivity, whereas Hall coefficient is insensitive to temperature and controlled by high carrier concentration. The role of substrate-induced disorder, which also promotes an insulating behavior as the two-dimensional limit is approached, is highlighted by comparing the properties of samples deposited on amorphous (quartz) and crystalline (sapphire) substrates. Our work demonstrates that the transport properties of $Bi_2Se_3$ films are highly tunable through finite-size effects which are of interest in applied areas such as nanoelectronics and spintronics.

## SUPPLEMENTARY MATERIAL

See supplementary material for an additional seven supporting figures (labeled S1-S7) and two tables (T1-T2).

## ACKNOWLEDGMENTS

[1]M. Z. Hasan and C. L. Kane, "Colloquium: Topological insulators," Rev. Mod. Phys. **82**, 3045 (2010).

[2]X.-L. Qi and S.-C. Zhang, "Topological insulators and superconductors," Rev. Mod. Phys. **83**, 1057–1110 (2011).

[3]D. Hsieh, D. Qian, L. Wray, Y. Xia, Y. S. Hor, R. J. Cava, and M. Z. Hasan, "A topological Dirac insulator in a quantum spin Hall phase," Nature **452**, 970 (2008).

[4]Y. Xia, D. Qian, D. Hsieh, L. Wray, A. Pal, H. Lin, A. Bansil, D. Grauer, Y. S. Hor, R. J. Cava, and M. Z. Hasan, "Observation of a large-gap topological-insulator class with a single Dirac cone on the surface," Nat. Phys. **5**, 398 (2009).

[5]H. Zhang, C. X. Liu, X.-L. Qi, X. Dai, Z. Fang, and S.-C. Zhang, "Topological insulators in $Bi_2Se_3$, $Bi_2Te_3$ and $Sb_2Te_3$ with a single Dirac cone on the surface," Nat. Phys. **5**, 438 (2009).

[6]D. Hsieh, Y. Xia, D. Qian, L. Wray, J. H. Dil, F. Meier, J. Osterwalder, L. Patthey, J. G. Checkelsky, N. P. Ong, A. V. Fedrov, H. Lin, A. Bansil, D. Grauer, Y. S. Hor, R. J. Cava, and M. Z. Hasan, "A tunable topological insulator in the spin helical Dirac transport regime," Nature **460**, 1101 (2009).

[7]F. Katmis, V. Lauter, F. S. Nogueira, B. A. Assaf, M. E. Jamer, P. Wei, B. Satpati, J. W. Freeland, I. Eremin, D. Heiman, P. Jarillo-Herrero, and J. S. Moodera, "A high-temperature ferromagnetic topological insulating phase by proximity coupling," Nature **533**, 513–516 (2016).

[8]G. J. Ferreira and D. Loss, "Magnetically defined qubits on 3D topological insulators," Phys. Rev. Lett. **111**, 106802 (2013).

[9]A. V. Kitaev, "Fault-tolerant quantum computation by anyons," Ann. Phys. **303**, 2–30 (2003).

[10]C. Nayak, S. H. Simon, A. Stern, M. Freedman, and S. Das Sarma, "Non-Abelian anyons and topological quantum computation," Rev. Mod. Phys. **80**, 1083 (2008).

[11]M. Dc, R. Grassi, J.-Y. Chen, M. Jamali, D. R. Hickey, D. Zhang, Z. Zhao, H. Li, P. Quarterman, Y. Lv, M. Li, A. Manchon, K. A. Mkhoyan, T. Low, and J.-P. Wang, "Room-temperature high spin-orbit torque due to quantum confinement in sputtered $Bi_xSe_{(1-x)}$ films" Nature Materials **17**, 800–807 (2018).

[12]M. T. Philip, M. R. Hirsbrunner, M. J. Park, and M. J. Gilbert, "Performance of topological insulator interconnects," IEEE Electron Device Lett. **38**, 138 (2017).

[13]S. K. Banerjee, L. F. Register, E. Tutuc, D. Reddy, and A. H. MacDonald, "Bilayer pseudo spin field-effect transistor (BiSFET): A proposed new logic device," IEEE Electron Device Lett. **30**, 158 (2009).

[14]N. Bansal, Y. S. Kim, M. Brahlek, E. Edrey, and S. Oh, "Thickness-independent transport channels in topological insulator $Bi_2Se_3$ thin films," Phys. Rev. Lett. **109**, 116804 (2012).

[15]M. Liu, C. Chang, Z. Zhang, Y. Zhang, W. Ruan, K. He, L. Wang, X. Chen, J. Jia, S. Zhang, Q. Xue, X. Ma, and Y. Wang, "Electron interaction-driven insulating ground state in $Bi_2Se_3$ topological insulators in the two-dimensional limit," Phys. Rev. B **83**, 165440 (2011).

[16]A. A. Taskin, S. Sasaki, K. Segawa, and Y. Ando, "Manifestation of topological protection in transport properties of epitaxial $Bi_2Se_3$ thin films," Phys. Rev. Lett. **109**, 066803 (2012).

[17]N. Bansal, Y. S. Kim, E. Edrey, M. Brahlek, Y. Horibe, K. Iida, M. Tanimura, G.-H. Li, T. Feng, H.-D. Lee, T. Gustafsson, E. Andrei, and S. Oh, "Epitaxial growth of topological insulator $Bi_2Se_3$ film on Si(111) with atomically sharp interface," Thin Solid Films **520**, 224 (2011).

[18]Y. S. Kim, M. Brahlek, N. Bansal, E. Edrey, G. A. Kapilevich, K. Iida, M. Tanimura, Y. Horibe, S.-W. Cheong, and S. Oh, "Thickness-dependent bulk properties and weak antilocalization effect in topological insulator $Bi_2Se_3$," Phys. Rev, B **84**, 073109 (2011).

[19]H. D. Li, Z. Y. Wang, X. Kan, X. Guo, H. T. He, Z. Wang, J. N. Wang, T. L. Wong, N. Wang, and M. H. Xie, "The van der Waals epitaxy of $Bi_2Se_3$ on the vicinal Si(111) surface: An approach for preparing high-quality thin films of a topological insulator," New J. Phys. **12**, 103038 (2010).

[20]J. H. Jeon, M. Song, H. Kim, W.-J. Jang, J.-Y. Park, S. Yoon, and S.-J. Kahng, "Quintuple layer $Bi_2Se_3$ thin films directly grown on insulating $SiO_2$ using molecular beam epitaxy," Appl. Surf. Sci. **316**, 42–45 (2014).

[21]A. Richardella, D. M. Zhang, J. S. Lee, A. Koser, D. W. Rench, A. L. Yeats, B. B. Buckley, D. D. Awschalom, and N. Samarth, "Coherent heteroepitaxy of $Bi_2Se_3$ on GaAs (111)B," Appl. Phys. Lett. **97**, 262104 (2011).

[22]C. L. Song, Y. Wang, Y. Jiang, Y. Zhang, C. Chang, L. Wang, K. He, X. Chen, J. Jia, Y. Wang, Z. Fang, X. Dai, X. Xie, X. Qi, S. C. Zhang, and Q. Xue, "Topological insulator $Bi_2Se_3$ thin films grown on double-layer graphene by molecular beam epitaxy," Appl. Phys. Lett. **97**, 143118 (2010).

[23]X. F. Kou, L. He, F. X. Xiu, M. R. Lang, Z. M. Liao, Y. Wang, A. V. Fedorov, X. X. Yu, J. S. Tang, G. Huang, X. W. Jiang, J. F. Zhu, J. Zou, and K. L. Wang, "Epitaxial growth of high mobility thin films on CdS," Appl. Phys. Lett. **98**, 242102 (2011).

[24]T. P. Ginley, Y. Wang, and S. Law, "Topological insulator film growth by molecular beam epitaxy: A review," Crystals **6**, 154 (2016).

[25]P. Orgiani, C. Bigi, P. K. Das, J. Fujii, R. Ciancio, B. Gobaut, A. Galdi, C. Sacco, L. Maritato, P. Torelli, G. Panaccione, I. Vobornik, and G. Rossi, "Structural and electronic properties of $Bi_2Se_3$ topological insulator thin films grown by pulsed laser deposition," Appl. Phys. Lett. **110**, 171601 (2017).

[26]Y. Onose, R. Yoshimi, A. Tsukazaki, H. Yuan, T. Hidaka, Y. Iwasa, M. Kawasaki, and Y. Tokura, "Pulsed laser deposition and ionic liquid gate control of epitaxial $Bi_2Se_3$ thin films," App. Phys. Exp. **4**, 083001 (2011).

[27]Y. Lin, Y. Chen, C. Lee, J. Wu, H. Lee, C. Liang, and Y. Chang, "A study on the epitaxial $Bi_2Se_3$ thin film grown by vapor phase epitaxy," AIP Adv. **6**, 065218 (2016).

[28]W. J. Wang, K. H. Gao, and Z. Q. Li, "Thickness-dependent transport channels in topological insulator $Bi_2Se_3$ thin films grown by magnetron sputtering," Sci. Rep. **6**, 25291 (2016).

[29]Y. Sapkota, A. Alkabsh, A. Walber, H. Samassekou, and D. Mazumdar, "Optical evidence for blue shift in topological insulator bismuth selenide in the few-layer limit," Appl. Phys. Lett. **110**, 181901 (2017).

[30]D. Kim, S. Cho, N. P. Butch, P. Syers, K. Kirshenbaum, S. Adam, J. Paglione, and M. S. Fuhrer, "Surface conduction of topological Dirac electrons in bulk insulating $Bi_2Se_3$," Nat. Phys. **8**, 459 (2012).

[31]D. Kong, J. J. Cha, K. Lai, H. Peng, J. G. Analytis, S. Meister, Y. Chen, H. Zhang, I. R. Fisher, Z. Shen, and Y. Cui, "Rapid surface oxidation as a source of surface degradation factor for $Bi_2Se_3$," ACS Nano **5**, 4698 (2011).

[32]M. Brahlek, Y. S. Kim, N. Bansal, E. Edrey, and S. Oh, "Surface versus bulk state in topological insulator $Bi_2Se_3$ under environmental disorder," Appl. Phys. Lett. **99**, 012109 (2011).

[33]J. G. Analytis, R. D. McDonald, S. C. Riggs, J. Chu, G. S. Boebinger, and I. R. Ficher, "Two-dimensional surface state in the quantum limit of a topological insulator," Nat. Phys. **6**, 960 (2010).

[34]S. S. Hong, J. J. Cha, D. Kong, and Y. Cui, "Ultra-low carrier concentration and surface dominant transport in antimony-doped $Bi_2Se_3$ topological insulator nanoribbons," Nat. Commun. **3**, 757 (2012).

[35]J. G. Analytis, J.-H. Chu, Y. Chen, F. Corredor, R. D. McDonald, Z. X. Shen, and I. R. Fisher, "Bulk Fermi surface coexistence with Dirac surface state in $Bi_2Se_3$: A comparison of photoemission and Shubnikov–de Haas measurements," Phys. Rev. B **81**, 205407 (2010).

[36]B. C. Park, T. Kim, K. I. Sim, B. Kang, J. W. Kim, B. Cho, K. Jeong, M. Cho, and J. H. Kim, "Terahertz single conductance quantum and topological phase transitions in topological insulator $Bi_2Se_3$ ultrathin films," Nat. Commun. **6**, 6552 (2015).

[37]A. R. Mellnik, J. S. Lee, A. Richardella, J. L. Grab, P. J. Mintun, M. H. Fischer, A. Vaezi, A. Manchon, E.-A. Kim, N. Samarth, and D. C. Ralph, "Spin-transfer torque generated by a topological insulator," Nature **511**, 449–451 (2014).

[38]J. Han, A. Richardella, S. A. Siddiqui, J. Finley, N. Samarth, and L. Liu, "Room temperature spin-orbit torque switching induced by a topological insulator," Phys. Rev. Lett. **119**, 077702 (2017).

[39]Y. Wang, D. Zhu, Y. Wu, Y. Yang, J. Yu, R. Ramaswamy, R. Mishra, S. Shi, M. Elyasi, K.-L. Teo, Y. Wu, and H. Yang, "Room temperature magnetization switching in topological insulator-ferromagnet heterostructures by spin-orbit torques," Nat. Commun. **8**, 1364 (2017).

[40]S. Cho, N. P. Butch, J. Paglione, and M. S. Fuhrer, "Insulating behavior in ultrathin bismuth selenide field effect transistors," Nano Lett. **11**, 1925 (2011).

[41]K. Momma and F. Izumi, "VESTA 3 for three-dimensional visualization of crystal, volumetric and morphology data," J. Appl. Cryst. **44**, 1272 (2011).

[42]S. Nakajima, "The crystal structure of Bi2Te3−xSex," J. Phys. Chem. Solids **24**, 479 (1963).

[43]J. Sun and D. J. Singh, "Using gapped topological surface states of $Bi_2Se_3$ films in a field effect transistor," J. Appl. Phys. **121**, 064301 (2017).

[44]Z. Li, S. Chen, J. Sun, X. Li, H. Qui, and J. Yang, "Spatial and thickness dependence of coupling interaction of surface states and influence on transport and optical properties of few-layer $Bi_2Se_3$," J. Phys.: Condens. Matter **30**, 065503 (2018).

[45]F. Schwierz, "Graphene transistors," Nat. Nanotechnol. **5**, 487 (2010).

[46]J. Wang, R. Zhao, M. Yang, Z. Liu, and Z. Liu, "Inverse relationship between carrier mobility and bandgap in graphene," J. Chem. Phys. **138**, 084701 (2013).

[47]D. Kim, Q. Li, P. Syers, N. P. Butch, J. Paglione, S. D. Sarma, and M. S. Fuhrer, "Intrinsic electron- phonon resistivity of $Bi_2Se_3$ in the topological regime," Phys. Rev. Lett. **109**, 166801 (2012).

[48]N. P. Butch, K. Kirshenbaum, P. Syers, A. B. Sushkov, G. S. Jenkins, H. D. Drew, and J. Paglione, "Strong surface scattering in ultrahigh-mobility $Bi_2Se_3$ topological insulator crystals," Phys. Rev. B **81**, 241301 (2010).